LAGRANGIAN DESCRIPTION AND FINITE ELEMENT ANALYSIS OF RELUCTANCE ACCELERATOR CIRCUIT MODEL

Gökhan DINDIŞ[1*]

[1]Eskişehir Osmangazi Üniversitesi, Mühendislik Mimarlık Fakültesi, Elektrik Elektronik Mühendisliği Bölümü, Eskişehir, ORCID No : http://orcid.org/ 0000-0001-5642-7212

Keywords

Lagrangian Description
Reluctance Accelerator
Electromagnetic Accelerator
Coil Gun
Electromagnetic Launcher

Abstract

Lagrangian description of electrical circuit model of a reluctance type accelerator system is introduced. The effectiveness of the general purpose magnetostatic finite element analysis (FEA) tools on the introduced model is demonstrated. Electrical equivalent circuit model of the system lays out many properties of the system in terms of voltage, current, power or energy distributions of electrical components, and also electrical equivalent of the mechanical components, in an easily perceivable form. These type of actuators are simple mechanisms when they are in steady state. However, when they are in transient, their dynamics may become very complex. The aim of the study is to show how this approach allows many researchers without the full electromagnetic background, to model and understand the dynamics of the reluctance type linear or rotary motor or actuators whether they are saturated or not. To exhibit the validity of the proposed model and solution of dynamic behaviors with FEA, it is verified on a basic capacitor discharge type driver circuit including the electromagnetic accelerator coil and projectile.

RELÜKTANS TÜRÜ İVMELENDİRİCİ DEVRE MODELİ İÇİN LAGRANGE TANIMLAMASI VE SONLU ELEMAN ANALİZLERİ

Anahtar Kelimeler

Lagrange Tanımlama
Relüktans Türü İvmelendirici
Elektromanyetik İvmelendirici
Bobin Silahı
Elektromanyetik Fırlatıcı

Öz

Relüktans türü ivmelendirici devre modeli için uygun bir Lagrange tanımı sunulmuştur. Magnetostatik sonlu eleman analizi yapan genel amaçlı programların, sunulan model üzerinde ne kadar etkin bir şekilde kullanılabileceği gösterilmiştir. Bir sistemin elektrik devre modeli, sistemi oluşturan parçaların davranışlarını, mekanik parçaların elektriksel eşdeğerleri de dahil olmak üzere akım, gerilim, güç ve enerji dağılımı gibi karşılıklarıyla kolay algılanabilir bir şekilde ortaya sermektedir. Bu tür tahrik sistemleri durağan çalışma şartlarında oldukça basit dinamiğe sahip olmakla birlikte geçiş durumlarında oldukça komplex davranış gösterirler ve çalışma dinamiklerinin anlaşılmaları güçtür. Çalışma, böyle bir yaklaşımın tam bir elektromanyetik alt yapıya sahip olmayan araştırmacılara doymuş veya doymamış relüktans tipi doğrusal veya dairesel hareket eden motor veya elektrikli tahrik sistemlerinin ve dinamik yapılarının daha iyi anlaşılabilmesi için yapılmıştır. Önerilen model ve dinamik davranışlarının sonlu eleman analizleri ile çözümü, bir relüktans ivmelendirici düzeneği gerçeklenip kondansatör boşaltmalı bir devre ile sürülerek doğrulanmıştır.

Araştırma Makalesi		Research Article	
Başvuru Tarihi	: 15.01.2020	Submission Date	: 15.01.2020
Kabul Tarihi	: 03.04.2020	Accepted Date	: 03.04.2020

1. Introduction

Using electromagnetic accelerators (EMA) to launch projectiles at high velocities has attracted researchers for more than a century. With the continuously emerging technologies, significant number of studies have contributed to the topic and have led to successively greater progress (McNab, 1999). Recent electronic and computational advancements have made it possible what was unimaginable previously. Yet, it seems there are fundamental issues still unknown to many researchers. Thanks to the newly developed affordable hardware and software tools so that more and more newcomers with different perspectives can step into this specific field and contribute even more. The well known survey paper on Electromagnetic Momentum (Griffiths, 2012) would be a good start point for detailed exploration for any type of magnetic

* Sorumlu yazar; e-posta : gdindis@ogu.edu.tr

accelerators.

EMAs may be classified under two categories. One of the categories can be described as railgun type accelerators which is not in the scope of this research. The second category on the other hand is coil gun type accelerators which has two subcategories: reluctance type and induction type. Both subcategories have some common features such as; one or more excitation coils located on a tubular runway or a barrel, and accelerating a projectile in the barrel to a high velocity with the thrust caused only by a magnetic field without any electrical contact. "Induction type accelerators" is not a subject to scope of this research, however these accelerators are far better than the reluctance type ones in regards of muzzle speed because practically no magnetic saturation problems they face as reluctance type ones do. An induction type EMA uses a non-ferrous but conductive sleeve type projectile. Thrust forces for this type of accelerators are based on the induction currents and Lorenz forces. Operational requirements of the induction types differ from the reluctance types and very high speeds (e.g. 2.5 km/s) are possible (Kaye, 2005). Also, some design procedures available in the literature which discusses for specific requirements of a super velocity launcher with 8 km/s muzzle speed (Balikci, Zabar, Birenbaum, and Czarkowski, 2007).

A reluctance type EMA uses a low reluctance projectile or sometimes called armature or slug that is energized by the magnetic field generated by one or more driver coils. For the reluctance type accelerators, the force that accelerates the projectile can be explained by Maxwell stress tensors. The quantitative calculation of the magnetic forces for any geometry and any projectile position can be done either by surface integral, the volume integral, or equivalent surface methods. Errors depend on the quality of the FEA solution but the volume integration methods are always more precise than the surface ones or the equivalent source ones (De Medeiros, Reyne, and Meunier, 1998). Analytical solution is very difficult and needs a lot of approximations but FEA tools yield reasonable accurate solutions for majority of cases. Limitations for the reluctance type accelerators seems still not well defined so far, and literature indicates much more research work can be done. One may say that simple search yields answers for these limitations easily. However, over hundreds of articles related to reluctance type accelerators, there was none that indicating a maximum reachable speed data with a physical verification. Literature indicates that induction and saturations are important factors for determining limitations of reluctance types, and directs the speed or energy seeking researchers to go for induction types. That might be the reason most of the researchers left the field without setting the approximated borders for key parameters like speed, energy or efficiency. That was the main motive to start for this research and therefore it is focused specifically on the reluctance type accelerators.

Before going into more detailed research a well defined model for the system is essential. There is a well known and established unified physical model for the reluctance type accelerators in the literature (Slade, 2005). A simplified physical model is developed from basic principles and cast in a Lagrangian form. However, in the model a longer armature than the coil has been taken into consideration and includes many simplifying assumptions. Some of those assumptions obviously fail with complex geometries, for example when the geometry has a bottleneck section. Another article from the same author introduces a fast finite element solver for a reluctance type accelerator which involves the writing the FEA program itself as a solver (Slade, 2006). Eddy currents and driving circuit elements are included in the model. However, for the more complex geometries it may not be a simple task for a researcher without the strong electromagnetic background, to write an electromagnetic finite element solver. A user friendly general purpose FEA program for magneto-static problems on the other hand, makes the process much simpler. So that, as proposed in this manuscript, a well defined electrical circuit equivalent model using a general purpose FEA toolset seems to be another way to go. There are articles and conference papers found in the literature look somehow similar to one proposed here. Some of them also use a general purpose FEA as a solver. However, simulations are far from close approximations since most of them don't even have projectile dynamics reflected on the electrical circuit models (Holzgrafe, Lintz, Eyre, and Patterson, 2012; Klimas,Grabowski, and Piaskowy, 2016; Khandekar, 2016).

2. Materials and Methods

2.1. Driver Coil

A driver coil is the essential part of an EMA. One, focusing on a single driver coil and modeling its physical behaviors on either stationary or moving projectiles obviously will encounter a multi-stage coil cases too. In fact, when a projectile comes to the first stage with a non-zero speed its behavior is not different than that in the following stages. Thus, examining a simple single stage driver coil is fundamental in understanding the mechanics of the operation. Copper is used generally for the coil material because of its good electrical conductivity properties. Besides, its wide industrial usage makes it low cost and available almost anytime. Windings should have a good insulation wire to wire and layer to layer. Stranded copper may add to the material cost but it is good for high frequency responses which specially needed at very high velocities. An efficient coil winding should have a high L/R ratio, unnecessary air pockets among the conductor wires should be avoided.

On the other hand, high L/R ratio makes the response time of the system very slow for the intended sudden development of the drive current and it becomes more difficult to drive the coil under low voltages and in a tight time frame. The inductance for a coil can be calculated as:

$$L = \frac{N^2}{\mathcal{R}} \quad (1)$$

where $\mathcal{R}$ is the total reluctance for the effected magnetic field. Relative permeability properties of the copper, air, fiber-glass, and plastic materials have almost the same as the vacuum has. Thus, if these are the main materials used for the coil and surroundings, the total reluctance is almost firm. When there is no saturation, for a given geometry, L strictly depends on square of number of turns N. Inside the conductor, L changes almost linear with N, but it has generally very small effect on the resulting L. To wind the same geometry with the same type of conductor; if the number of turns N needs to be increased, wire diameter should be decreased to fit into the volume, or vice versa. If the diameter of the wire decreases its ohmic resistance R increases as L does. As a result, time constant L/R stays almost the same. However, changing the air/conductor ratio by winding with some air gaps is a different issue. Introducing a material with a lower reluctance into the field also effects the overall permeability by increasing the inductance, and the L/R ratio accordingly. This happens exactly when a ferrous projectile breeches the coil.

2.2. Projectile

Magnetic coupling between the coil and the projectile should be maximized for a good power transfer. Therefore, coil design and projectile design has to match each other in sizes, in weights, and so on. For the reluctance type EMAs the projectile material should have good magnetic permeability. Magnetic saturation reduces the magnetic permeability of the material at elevated current values, and therefore it should be avoided as much as possible for the overall efficiency. A simple projectile can be made from a piece of soft iron or ferrous steel, which is cylindrically shaped to fit the bore of the barrel with a smallest air gap. However this kind of material will have its own limitation due to high eddy currents. Eddy currents have negative effects on projectile's speed and efficiency. Lorentz forces created by eddy currents create force in the negative direction when projectile is supposed to be pulled towards the center of the coil. If the material's ohmic resistance is low, then the force will be stronger and will last longer. If the ohmic resistance is moderate, it will allow eddy currents for a shorter time frame by converting the power to the ohmic losses. High electrical resistance of the projectile material is preferred due to minimizing the eddy currents. Soft ferrites made out of sintered powders contain iron oxides combined with nickel, zinc, and/or manganese have high resistivity against the eddy currents. However their permeability is considerably lower than solid or stacked ferrous materials; that's why they perform poorly (Slade, 2005). Experiences indicate that, for the low speed coil stages mainly low permeability and better magnetic saturation specs are required.

Geometry of the projectile is also important. Length for example, can be optimized to maximize the energy or speed of the projectile (Daldaban and Sarı, 2016).

2.3. Driving Circuit

For the coil driving generally voltage-source type power supplies are used. Obviously, they should have high current capabilities and fast response times for the purpose. This can be done easily by connecting large capacitor banks parallel to the output of the power supply. That makes the impedance of the output of the power supply, in contrast to the coil impedance, much lower. Switch internal resistors also should be very small, and for the same reason hook-up wires should be kept short and thick.

Silicon controlled rectifiers (SCR) are commonly used for energizing the coils. Their high current and voltage ratings and low internal resistivity makes them good choices for this purpose. Capacitor or capacitor-bank types discharge circuits are suitable for the operation. A simple circuit example can be given as in Figure 1 (a). The capacitor should have the right energy to dump to the coil, so there would be no suck back effect beyond the center position. Because a standard SCR naturally will not turn off until the current reaches zero. A gate turn off thyristor (GTO) can be a solution (Rashid, 2011), but going into that direction is not much different than using MOSFET or IGBT. In normal operation, when the projectile is in the pull zone and SCR is set on, current starts to accelerate the projectile toward the center of the coil. The total electrical energy left in the capacitor and the coil itself should be equal to zero as soon as the projectile reaches the center. Otherwise, current will be still flowing, and the projectile will start to decelerate.

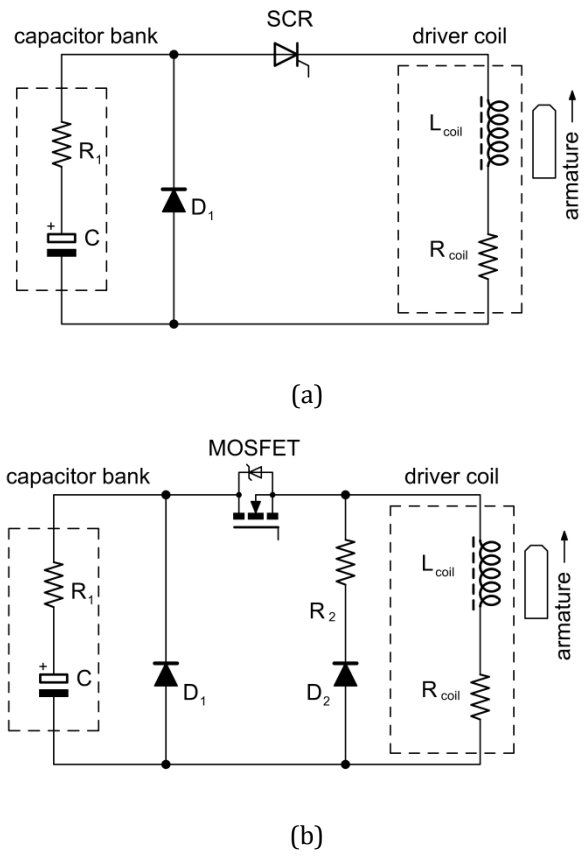

Figure 1. Simple SCR (a) and MOSFET (b) Controlled Circuits for Capacitor Discharge Type Coil Driving

Metal oxide silicon field effect transistors (MOSFET) or isolated gate bipolar transistors (IGBT) are also commonly used for energizing the coils. We will use the term transistor for both type of switches in this section. Their high current, voltage, and low internal resistance values cannot not compete with the SCRs', however their high switching-on and switching-off properties give users a better control than a SCR can offer. In a simple use, when the transistor is turned off while some current is still passing through, a fly-wheel diode D2 and a quenching resistor may handle the turn-off inductive high voltage spike and protect the transistor from getting damaged (Figure 1 (b)). A snubber circuit parallel to the transistor switch is also advised if long hook-up wires used. In transistor controlled systems one big capacitor-bank can be used for repetitive shots or multi coil driving purposes. Diode D1 is for the the purpose of preventing electrolytic capacitors from charging backward which may harm the capacitors in the time thereafter.

2.4. Principles of Operation for the Reluctance Type Accelerator

The physical principle of the operation for the reluctance type accelerators can be explained in simple terms. A magnetic field is a force field for a low reluctance material. The material has tendency to move into the direction of lowering the reluctance of the magnetic field. Considering this, following actions are taken to accelerate the projectile to the desired speed. A temporary magnetic field is generated in the coil by applying a current through the coil. Naturally, the projectile is forced to move to the center of the coil, since there is potential for lowering the reluctance in that direction. It accelerates until the center point where reluctance is the lowest and speed is the maximum. After this point current should be suddenly cut off and temporary magnetic force field should be vanished as soon as possible. Otherwise the force field is going to pull the projectile back to the center. After switching the current off, a small, short lasting suck back effect might be permitted, since its decelerating effect is minimal and making it completely disappearing is a challenging task.

2.5. The Lagrangian Model

A simplified electrical circuit model for a reluctance type accelerator is given in Figure 2. The voltage source stands for the capacitor bank used to drive the circuit. The total equivalent resistance R includes capacitor's internal resistance, switch-on resistance and coil resistance all combined. The inductance $L(x, I)$ represents inductance of the coil which changes as a function of projectile position and current flowing through the coil. Because of the high ampere-turn ratios projectile goes to magnetic saturation and it is obvious for L to be function of I. The last part in the model represents the effect of the projectile's mechanical properties. The projectile is magnetically coupled to the circuit and its effect on the circuit will change significantly by its dynamic and physical parameters. Magnetic force $F(x, I)$ applied to the projectile changes also by its position in the coil due to the degree of the magnetic coupling. On the other hand a moving projectile changes the magnetic reluctance and therefore changes the magnetic flux in the magnetic circuit as well. It is well known that according to the Faraday's law, changing flux over the time induces voltage on the coil it passes through. This phenomenon taking place is the generator effect and it is observed in any kind of motor or electro-mechanical actuator motion. That's why a counter electromotive force (or back-emf) should exist in the electrical circuit models too.

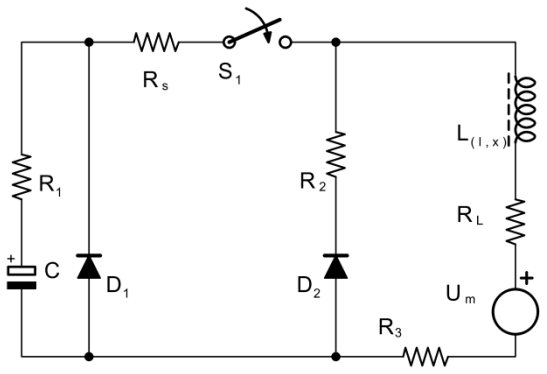

Figure 2. Electrical Circuit Model

There will be some induction currents on a solid iron or steel projectile. It is at neglectable levels for low slew rate current applications, but naturally rises up with the high slew rate current pulses required in the following coil stages. This induction will cause large Lorentz forces in negative direction during the breeching phases of the projectile. So, modeling for the high speed coil stages will be another challenging problem and it is not in the scope of this manuscript. Projectiles subject to fit the model proposed in this paper are assumed either running at low speed applications (less than about 50 m/s) or they have geometries to reduce the induction currents as in slitted solid projectiles (Barrera and Beard, 2014) or projectiles made from laminated sheets or wire/epoxy cores (Slade, 2005).

The Lagrangian of an electromechanical system $\mathcal{L}$, in a general sense, takes the form as in Equations (2)–(5) (Slade, 2005; Goldstein, Poole, and Safko, 2002).

$$\mathcal{L} = \mathcal{T} - \mathcal{V} \tag{2}$$

$$\mathcal{T} = T_L + T_m \tag{3}$$

$$\mathcal{V} = V_C \tag{4}$$

Where T_L and T_m are kinetic energy of the inductor and projectile respectively, V_C is the potential energy of the capacitor. In expanded form they are shown in Equations (5)-(7).

$$T_L = \tfrac{1}{2}L(\dot{q},\dot{x})\dot{q}^2 \tag{5}$$

$$T_m = \tfrac{1}{2}m\dot{x}^2 \tag{6}$$

$$V_C = \tfrac{1}{2}\frac{q^2}{C} \tag{7}$$

where m and x are mass and position of the projectile, and q is the charge of the capacitor. Then, including the dissipative term $R\dot{x}$, equations of motion can be expressed separately as in Equations (8)-(9), for the electromotive forces (emf) and mechanical forces respectively.

$$\frac{d}{dt}\left(\frac{\partial \mathcal{L}}{\partial \dot{q}}\right) - \frac{\partial \mathcal{L}}{\partial q} + R\dot{q} = U_p \tag{8}$$

$$\frac{d}{dt}\left(\frac{\partial\left(\frac{1}{2}m\dot{x}^2\right)}{\partial \dot{x}}\right) = F(\dot{q},x) \tag{9}$$

where U_p is the electromotive force field effect at the magnetic coupling of the moving projectile that is seen at the electrical circuit side and R represents the total circuit resistance. Then, Equation (8)-(9) yields Equations (10)-(11).

$$-\frac{q}{C} + L(\dot{q},x)\ddot{q} + \frac{\partial L(\dot{q},x)}{\partial \dot{q}}\dot{q}\ddot{q} + \frac{dL(\dot{q},x)}{dt}\dot{q} + \tfrac{1}{2}\frac{d}{dt}\frac{\partial L(\dot{q},x)}{\partial \dot{q}}\dot{q}^2 + R\dot{q} = U_p \tag{10}$$

$$m\ddot{x} = F(\dot{q},x) \tag{11}$$

When induction, hysteresis, and friction losses are all in neglectable amounts, conservation of the power for the electromagnetic coupling yields Equation (12).

$$U_p\dot{q} + F(\dot{q},x)\dot{x} = 0 \tag{12}$$

In plain words, whatever the power amount electromotive force supplies to the coupling has to be received by the mechanical system and should be turned into mechanical power and vice versa. The equations are unified as shown in Equation (13).

$$-\frac{q}{C} + L(\dot{q},x)\ddot{q} + \frac{\partial L(\dot{q},x)}{\partial \dot{q}}\dot{q}\ddot{q} + \frac{dL(\dot{q},x)}{dt}\dot{q} + \tfrac{1}{2}\frac{d}{dt}\frac{\partial L(\dot{q},x)}{\partial \dot{q}}\dot{q}^2 + R\dot{q} + \frac{1}{\dot{q}}F(\dot{q},x)\dot{x} = 0 \tag{13}$$

Finally, when $\dot{q}$ and $\frac{dL(\dot{q},x)}{dt}$ are replaced by I and $\frac{dL(I,x)}{dx}\dot{x}$ respectively, the equation becomes:

$$-U_c + L(I,x)\frac{dI}{dt} + \frac{\partial L(I,x)}{\partial I}I\frac{dI}{dt} + \frac{dL(I,x)}{dx}I\dot{x} + \tfrac{1}{2}\frac{d}{dt}\frac{\partial L(I,x)}{\partial I}I^2 + RI + \frac{F(I,x)}{I}\dot{x} = 0 \tag{14}$$

Equation (14) clearly lays out the important properties of the system. First of all, the Equation 14 is nothing

different than the Kirchhoff's voltage law. The $\frac{\partial L(I,x)}{\partial I}$ in the equation appears to be representing the magnetic saturation effect and it is neglectable at currents of non-saturating levels. The term $\frac{F(I,x)}{I}\dot{x}$ which may be expessed as $\frac{F(I,x)}{I^2}I\dot{x}$ as well, causes some of the back-emf voltage which is a natural response of the projectile moving in the coil. Some back-emf voltage is also produced by its co-energy counterpart $\frac{dL(I,x)}{dx}I\dot{x}$. Until the saturation point, ratio $\frac{F(I,x)}{I^2}$ follows a constant curve and it gets smaller with the increasing saturation level. Figure 5 (a) and (b) in section 4.2 demonstrate this illustratively. Note that, if we denote

$$K_m = \frac{F(I,x)}{I^2} \tag{15}$$

then, the term $\frac{F(I,x)}{I^2}I\dot{x}$ becomes equal to $K_m I\dot{x}$ for the smaller linearized sections, and it is proportional with the coil current or projectile speed. This is a typical DC motor/generator behaviour. When the speed is constant more excitation current produces more voltage, and when excitation current is constant more speed produces more back emf voltage; which is not surprising. The other terms in Equation (15), $\frac{\partial L(I,x)}{\partial I}I\frac{dI}{dt}$ and $\frac{1}{2}\frac{d}{dt}\frac{\partial L(I,x)}{\partial I}I^2$ appear to be representing the electro-motive force introduced by the saturating effect of the magnetic field. U_m in Figure 2 represents emf responses of the terms related to the moving projectile. In a motion of acceleration with a proper current flow; projectile builds more kinetic energy while speeding up, but coil builds more magnetic energy too as its inductance also increases. Naturally, as power consumers, during this kind of process they both put their responses to the circuit as electro-motive force effects. If all the equations are re-organized we get the differential equations below:

$$\frac{dI}{dt} = \frac{U_c - \frac{dL(I,x)}{dx}I\dot{x} - \frac{1}{2}\frac{d}{dt}\frac{\partial L(I,x)}{\partial I}I^2 - RI - \frac{F(I,x)}{I}\dot{x}}{L(I,x) + \frac{\partial L(I,x)}{\partial I}I} \tag{16}$$

$$\frac{dU_c}{dt} = -\frac{1}{C} \tag{17}$$

$$\frac{d^2x}{dt^2} = \frac{1}{m}F(I,x) \tag{18}$$

These differential equations (Equations (16)-(18)) can be solved by numerical analysis methods iteratively for given $F(I,x)$ and $L(I,x)$ values. An FEA tool comes handy to obtain these values, since it gives us magneto-static solutions for any given current and position values. Section 4 describes how exactly it can be done.

2.6. Finite Element Analyses

The finite element analysis is basically a numerical method for finding approximate solution to boundary value problems in partial differential equations. It subdivides a large problem into smaller, simpler parts that are called finite elements. When these finite elements define the model of the entire system behavior well enough, assembled simple solutions of these small, simple elements will yield approximate solution for the entire model of the system. When elements are chosen much smaller, naturally approximations gets more accurate but computation time gets enormously longer.

2.7. Initial Analyses with FEMM: Inductance and Force Responses of the Coil with a Projectile

In this article a public licensed "FEMM" software is used which gives simple planar or axisymmetric solutions for magneto static problems. There are many research examples in the literature using this software as their main tool (Klimas at al., 2016; Baltzis, 2010). It offers solutions for planar and axisymmetric problems (Meeker, 2004). A simple axisymmetric geometry of a coil and projectile can be easily drawn and solutions can be calculated as in Figure 3. Geometry is drawn in cross sectional form. Since it is cylindrically rotated around the central axis, drawing only one half of the cross section of the geometry will be just enough. Results can be displayed or exported in graphical or numerical form. It has a build-in library for many magnetic and conductive circuit materials. If the properties of the materials are chosen or edited correctly, even with default mesh size, errors are generally in single digit percents or less. When the system has non-symmetric structure, then, any of those 3D FEA software packages can be used for the solutions.

Solving the Lagrange equations requires solving of $F(I,x)$ and $L(I,x)$ data for any given current value at any given projectile position. However, before jumping straight to the solution of the dynamic problem, doing some static analyses is very helpful. This gives us some sense about the behavior of the system. In any FEA suitable for this purpose, the geometry can be drawn and simulated calculations can be recorded. In FEMM, the geometry is animated step by step, or mm by mm, and results can be recorded automatically via a companion script language tool, called Lua . The procedural steps are itemized below for obtaining the finite number of $F(I,x)$ and $L(I,x)$ data for the range of interest.

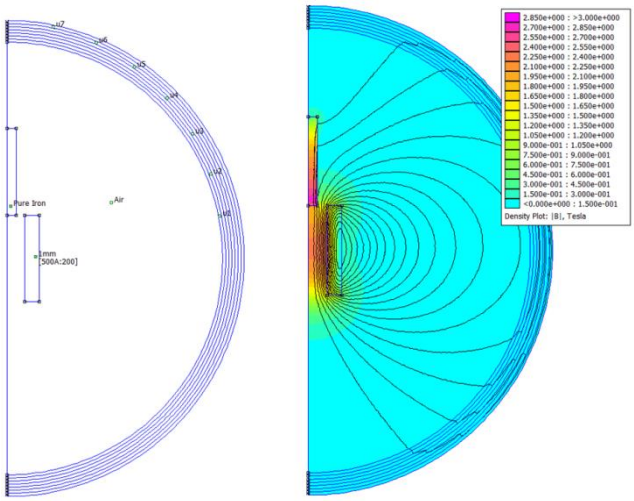

Figure 3. Axisymmetric FEA Model of Coil with Entering Projectile (left) and Field Solutions

FEMM Procedure to obtain the current responses

- Define the materials to be used. Import from libraries if they are already defined, and modify if needed
- Draw the geometries for initial position
- Define the boundaries
- Write a code in Lua script language for iterating the process N times for ;
  - analyzing and displaying the output fields,
  - calculating "Weighted Maxwel Stress Tensor Force" value,
  - calculating equivalent "Inductance" value, recording the values on a file,
  - advancing projectile 1mm further towards the muzzle direction
- Execute the Lua code

Results verify that when projectile is at the entrance the inductance is minimum and when it is right at the center it reaches the maximum. Inductance change per distance at a constant current level appears to be determining the force, which also makes sense. When this ratio is at the maximum the force is also at the maximum. If the ratio is zero then so is the force. In fact, force becomes zero in two cases; the first case is when the projectile is right in the middle and the second is if the projectile is at the infinity. Therefore, we see non-zero values at both entrances as shown in FEMM analysis graphs in Figure 4 (a). The reason is that the reluctance of the projectile at the entrance still effects the total reluctance in some small amounts. One more detail needs to be mentioned; that is the direction of the force. Since the reluctance becomes lower towards the center, in this type of accelerators the main force direction is always toward to the center of the coil (Figure 4 (b)). Thus, when accelerated projectile passes the center the force becomes negative (slows the armature down). Energy will be transferred from the armature back into the magnetic field.

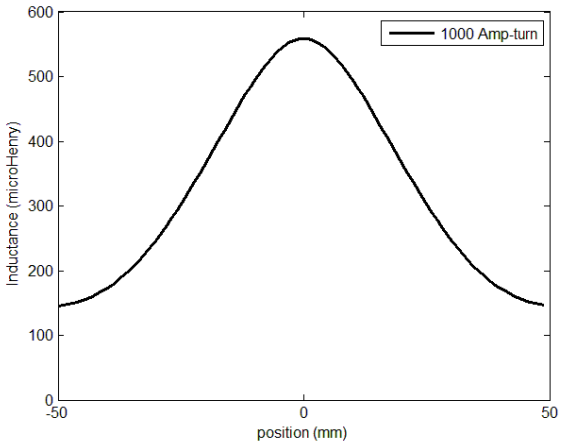

(a)

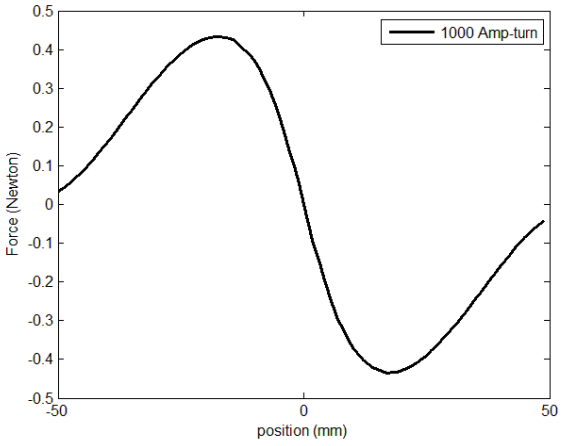

(b)

Figure 4. Typical Inductance (a) and Force (b) Results via FEMM Analyses

Because of the magnetic saturation properties of the projectile, its B-H curve will be almost linear up to a certain current level, but after that point, it will start to act nonlinearly. Therefore, more FEMM analyses have to be done with different current values until and after the saturation, so that the effects become visible and the behavior of the system due to saturation can be observed and commented.

The graphical results for the data in Table 1, for the coil-projectile setup, are shown in Figure 6 (a) and Figure 6 (b). These comparative figures demonstrate the

saturation effects on forces for different current values. Figure 6 (a) shows the force graphs for different current values. More force levels for higher currents are still possible after the saturation. But the force levels will not be proportional with square of the current I anymore. It is clearly seen in Figure 6 (b) that normalized force graphics for 1000 amp-turns and 2500 amp-turns are almost identical at unsaturated current levels. Furthermore, at saturated current levels, increasing the current starts to move the peaks of the curves from the center toward the entrance of the coil. The tools used in regular FEMM simulations are made for magneto-static problem solving, therefore induction or eddy currents, hysteresis effects, skin effects etc. are not accounted. These effects are generally not in considerable amounts at low speeds and will cause minor differences in the results.

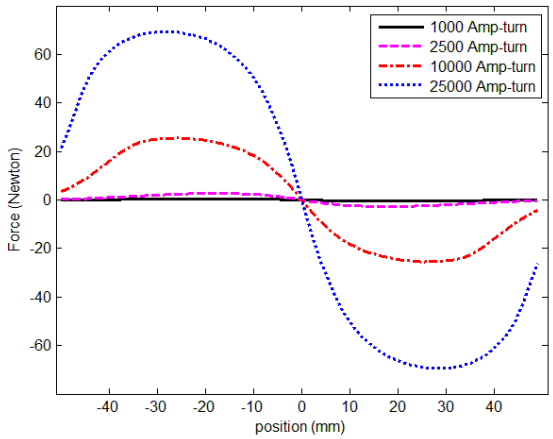

(a)

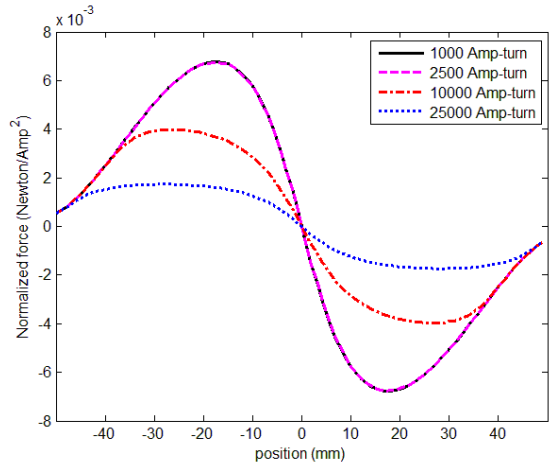

(b)

Figure 5. Force Data (a) and Normalized Force Data (b) of FEMM Results

Table 1. Parameters Used in Simulation

variable	value	Units
C	0.0705	Farads
R_1	0.015	ohms
R_L	0.11	ohms
N (number of turns)	125	turns
d_1 (internal dia. of the bobbin)	21	mm
l_1 (internal length of the	48	mm
a_1 (wire diameter)	21	mm
R_2	0.25	ohms
R_3	0.0025	ohms
R_s (switch and hook-up wire	0.01	ohms
l_2 (projectile length)	50	mm
d_2 (projectile diameter)	10	mm
m (mass)	30	grams
U_c (initial cap. voltage)	50	volts
I_i (initial inductance current)	0	amperes
x (initial position)	-48	mm
v (initial velocity, $\dot{x}$)	0	m/s

2.8. Simulation of Lagrangian Model with the Integrated FEMM Software

For the verification purpose of the proposed Lagrangian model of the system, the simple circuit model in Figure 2 is taken into consideration. This made experimental setup easy to implement too. Parameters are given in Table 1. For the current sensing four parallel connected 0.01 ohm resistors are used. Five paralleled IRFP064 MOSFETs used as a switch in the experimental circuit and catalog on-resistance value for each one shows 9 milliohms, if they are driven properly. So, equivalent switch resistance makes about less than 2 milliohms.

In FEMM, by using the companion scripting language Lua, it is straightforward to collect $F(I,x)$ and $L(I,x)$ data with given I, and x values. So, analyzing the coil behaviors under saturation conditions becomes possible by the simulation. The Lua language is a "MATLAB" like scripting language. Solving the differential equations of the model is possible iteratively, by solving magnetic circuit via FEA 'on the go'. The following procedure explains how it can be done:

FEMM Procedure for Solving the Equations of the Motion:

For the magnetic circuit;

- Define the materials to be used. Import from libraries if they are already defined, and modify if needed
- Draw the geometries for initial position
- Define the boundaries

For Lagrangian model;

- Define the parameters capacitance C, resistance R, projectile mass m

- Define the initial conditions for , $I, x, \dot{x}$
- Start with time t = 0 (time frame k = 0)

To iterate for the desired time period;

- Solve magnetic circuit, obtain $F(I,x)$ and $L(I,x)$
- Solve magnetic circuit again, this time for the partial derivatives via small variations
- Solve differential equation, obtain k_{th} time frame values
- Save k th time frame values
- Update the position x and current value I in the magnetic circuit for the next time frame
- Update time t, and time frame k ($t \leftarrow t+\Delta$, $k \leftarrow k+1$)
- Repeat iteration until reaching the desired condition

3. Case Studies and Findings

3.1. Case Study 1: Simple Capacitor Discharge

To evaluate the behaviour of the dynamic system for a simple capacitor discharge, a Lua script file is prepared and executed according to the procedure given to solve the equations. The results are recorded in a text file and drawn by using MATLAB graphical tools. The iteration started at the position -48mm and continued for 10 milliseconds with 0.1 millisecond time steps.

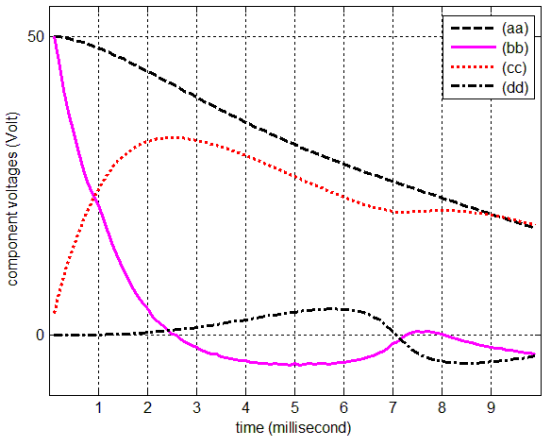

(a)

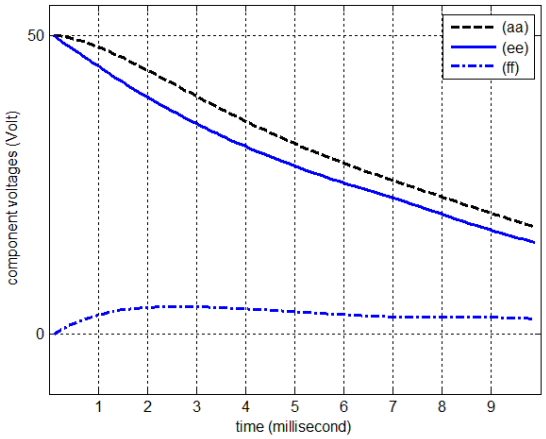

(b)

Figure 6. Component Voltages

The outputs are rewarding. From the electrical circuit model point of the view, graphical illustrations clearly lays out dynamic behavior of the reluctance type accelerator (Figure 6 (a) and (b)). Curve “aa” shows the capacitor voltage change during the discharge. It is apparent that, each component of the circuit model of the coil reacts with its own unique dynamic behavior. Inductive component “bb” and resistive component “cc” of the coil clearly dominate among the rest and demonstrate the largest voltage swings. Note that resistive component voltage changes linearly with the current and has a peak around t = 2.6ms. After that peak, when current value starts to decrease, inductive component starts to act as generator and try to keep current steady. That’s why its voltage changes the polarity and continues that way until current starts to increase again around t=7 ms. At this point the projectile is basically just after the middle point and because of the suck back effect of the coil it gives some of its kinetic energy back to the system. It is nice to observe that, some of the energy shows itself as increasing current effect. Of course increasing the current means also increasing the energy of the inductive component. Obviously some big portion of the energy becomes heat at the resistive component. When we look at the curve “dd”, we see the moving projectile’s responses. This response is called as “back electromotive force” of the projectile just like in the rotary DC motors. As it speeds up, more voltage drops will be seen. However, close to the middle of the coil, there is not much magnetic potential differences, so we lose the emf effect of the projectile. Beyond the middle point the direction changes the other way around, and we see the projectile as an energy source. When it gives energy back to the system, sometimes the contribution may not be enough to increase the current but at least slows the current reduction rate. In the accelerator this is not a desired situation, since the main goal is to keep increasing the

kinetic energy or the speed of the projectile. The curve "ee" on Figure 6 (b) shows the total coil voltage which could be measured from both ends of the physical coil. Some voltage drops will be in the internal resistors of the capacitors and switch components, and that effect is also seen as curve "ff".

Force and velocity graphics of the results are given in Figure 7. After the middle point (around t = 7.2 ms), force direction changes and projectile start to lose its speed. It is clearly seen that force is very high around t = 4 ms. Since some of the energy is gone for the resistive losses, suck back effect around t = 8.7 ms is not high as it was at the beginning. As a result, projectile will still have some speed while exiting the force field. The simulation results of the model reveals a good supporting information.

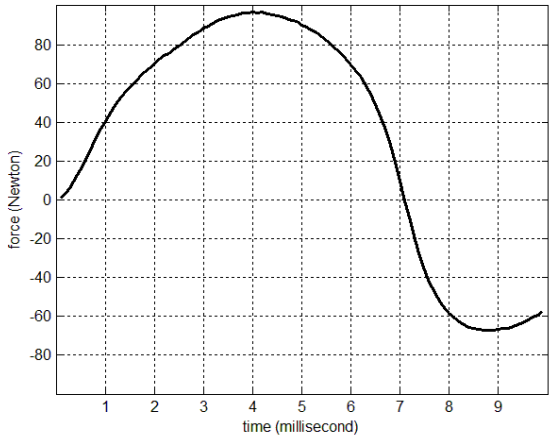

(a)

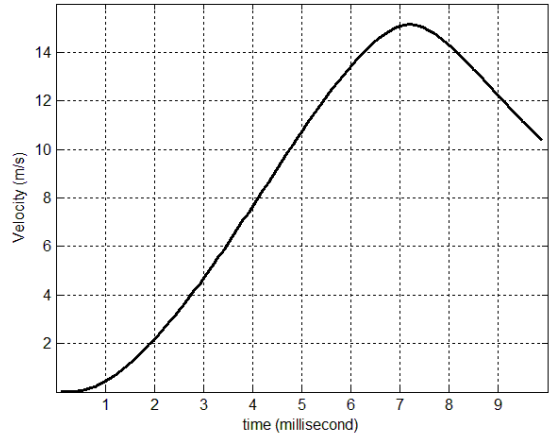

(b)

Figure 7. Force (a) and Velocity (b) Outputs

3.2. Case Study 2: Sensor Controlled Capacitor Discharge

As a second case study, simulations are done for the controlled discharge situations. Assumed that discharge event started by turning the switch on when the projectile is at the entrance, and switch off when the projectile is reached the center. Formulation of the Lagrange model slightly changed when the control switch is off; capacitor is taken out of the equation and extra resistor is added in series with an ideal fly-back diode. Two sub-cases are evaluated; one is with a zero ohm resistor value, and the other one is with a proper value to act like a quenching resistor. Since the current rates might be quite high, we can not choose a big value to create excessive voltage spikes. The one with fly-back diode alone (Figure 8(a)) demonstrated a little higher suck back effect than the other one (Figure 8 (b)), just as expected.

Scientific and publication ethics guidelines are followed in all phases of this study.

3.3. Experimental Work

For the verification of the proposed model a simple apparatus has been prepared mechanically as shown in Figure 9. System has an acrylic barrel as a runway. The coil specifications are same as those used in the simulation so that the comparisons make a quite sense. Position sensor made out of an infrared LED and photo-transistor pair and used for detecting when the projectile is at the center. Since it is located at the entrance and projectile length is equal to the coil length, as soon as projectile passes the sensor the switch can be turned off. Speed sensors are made out of two optical sensors placed 10 mm apart and located after the coil. A micro-controller is used for controlling of the entire operation. The capacitor bank is charged to 50V, the switch is turned on by pushing the fire button to start discharging the capacitor bank into the coil, and let the current flowing until the projectile reaches the coil center. Then, while projectile is exiting the coil the muzzle speed is measured by using the time delay between two sensor signals. All experiments are repeated numerous times. Coil voltage and current values are recorded by using a storage oscilloscope. The muzzle velocity values are also recorded for each experiment.

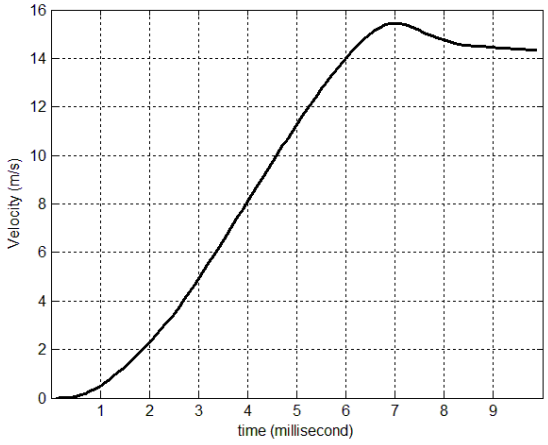

(a)

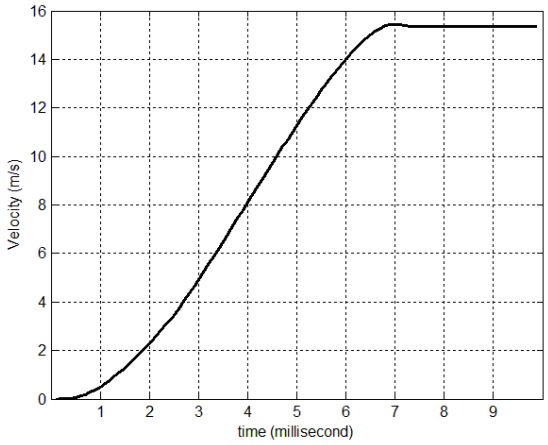

(b)

Figure 8. Velocity Graphics for Fly-back Diode Alone (a) and with Quenching Resistor (b)

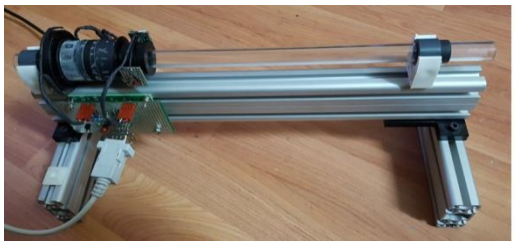

Figure 9. Single Stage Experimental Setup (a) and Used Projectile (b)

4. Discussions

Results are very similar to the ones obtained through the simulations. Figure 10 (a) and (b) show the current and voltage values. Magnitudes of simulation coil currents and muzzle velocities are close but slightly higher than experimental ones. Waveforms of the signals show exactly the same behavior. The muzzle speeds are 10.2 m/s and 9.1 m/sn (averaged) obtained by the simulation and real measurements respectively. Figure 11 and Figure 12 shows sensor controlled cases of the experiment results and the simulation results. The velocity obtained at case 2b is again slightly higher than the velocity obtained at case 2a as expected.

The simulated velocity results for the case 2a and 2b are 14.4 m/s and 15.3 m/s, and measured ones are averaged around 12.2 m/s and 13.1 m/s, respectively. There is a very important point here to be mentioned; since the solid projectile acts like a transformer's secondary by itself, induction occurs for high *dI/dt* rates even in the armature itself. Therefore, quenching the primary circuit (the coil itself) does not take the energy of the magnetic field right away. Note that, in the proposed model induction currents are not taken into account. The nonlinear semiconductor effects during the quenching time is not taken into account either.

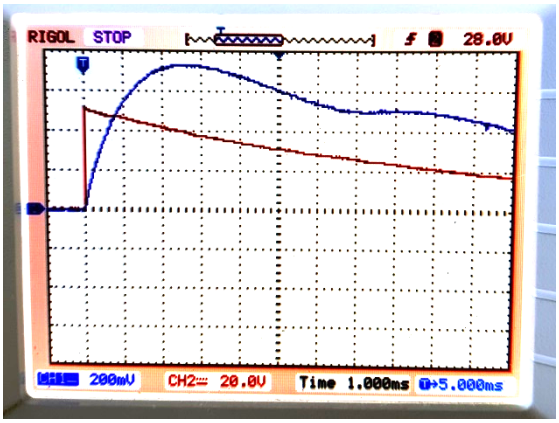

(a)

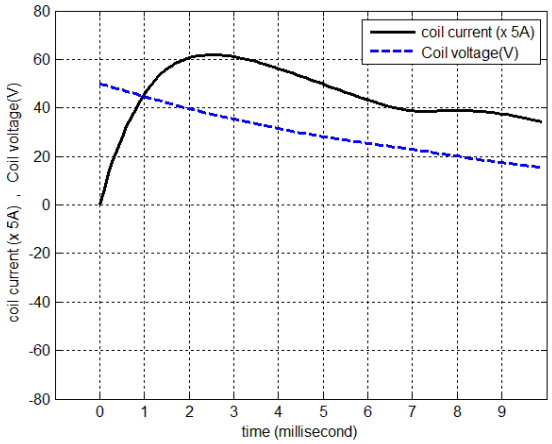

(b)

Figure 10. Measurement and Simulation Results for Case 1

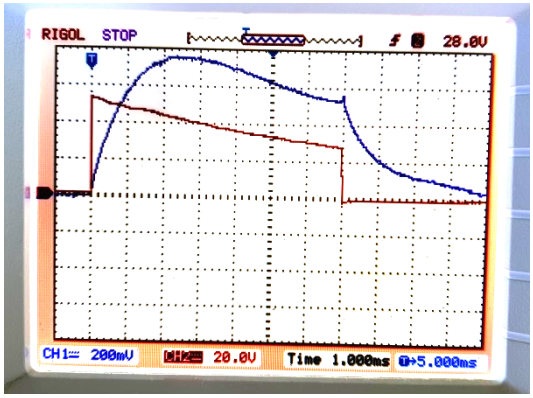

(a)

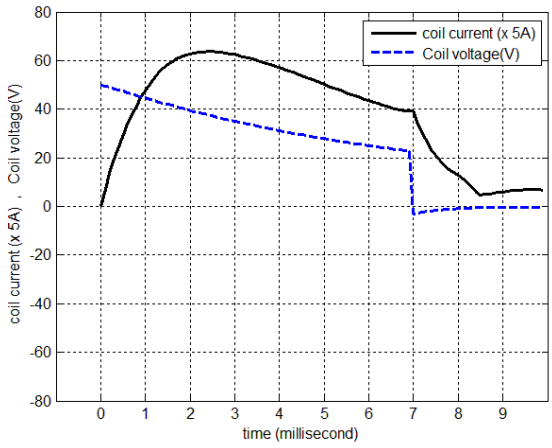

(b)

Figure 11. Measurement and Simulation Results for Case 2a

(a)

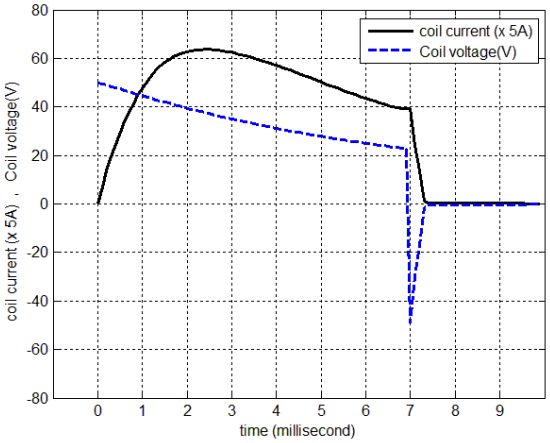

(b)

Figure 12. Measurement and Simulation Results for Case 2b

5. Conclusions

A well suited Lagrangian derived electrical circuit model for a reluctance type magnetic accelerator is introduced. With the electrical circuit model, each component's behavior can be studied individually to understand the whole. For the geometries with more complexity, using a user friendly general purpose FEA program for magnetostatic problems makes this kind of problems easy to deal with. Proposed model with the use of general purpose FEA tool might be another preferred way to go for the engineers without a strong electromagnetic background. When the parameters are entered correctly, model offers accurate equations of the motion. A single stage accelerator is evaluated by simulations and a physical system setup. Results obtained by the simulations and the actual experiments verify the effectiveness of proposed model and toolset for the low speed reluctance type accelerators.

Conflict of Interest

There is no conflict of interest.

References

Balikci, A., Zabar, Z., Birenbaum, L. & Czarkowski, D. (2007). On the design of coilguns for super-velocity launchers. *IEEE Transactions on Magnetics*, 43(1), 107-110. doi: http://doi.org/10.1109/TMAG.2006.887651

Baltzis, K. B. (2010). The finite element method magnetics (FEMM) freeware package: may it serve as an educational tool in teaching electromagnetics?. *Education and Information Technologies*, 15, 19-36. doi: https://doi.org/10.1007/s10639-008-9082-8

Barrera, T. & Beard, R. (2014). Exploration and verification analysis of a linear reluctance accelerator. *17th International Symposium on Electromagnetic Launch Technology (EML)*, La Jolla, CA, USA. doi: https://doi.org/10.1109/EML

Daldaban, F. & Sarı, V. (2016). The optimization of a projectile from a three-coil reluctance launcher. *Turkish Journal of Electrical Engineering & Computer Sciences*, 24, 2771-2788. doi: https://doi.org/10.3906/elk-1404-18

Griffiths, D. J. (2012). Resource letter em-1: electromagnetic momentum. *American Journal of Physics*, 80(1), 7-18. doi: https://doi.org/10.1119/1.3641979

Goldstein, H., Poole, C. P. & Safko, J. L. (2002). *Classical mechanics*. Pearson.

Holzgrafe, J., Lintz, N., Eyre, N. & Patterson, J. (2012). Effect of projectile design on coil gun performance. *Franklin W. Olin College of Engineering*.

Kaye, R. J. (2005). Operational requirements and issues for coilgun electromagnetic launchers. *IEEE Transactions on Magnetics*, 41(1), 194-199. doi: https://doi.org/10.1109/ELT.2004.1398047

Khandekar, S. (2016). Single-stage reluctance type coilgun. *International Journal of Recent Research in Electrical and Electronics Engineering (IJRREEE)*, 3(3), 31-36.

Klimas, M., Grabowski, D. & Piaskowy, A. (2016). Efficiency analysis of an electromagnetic launcher. *Elektryka, Silesian University of Technology Publishing*, Poland.

McNab, I. R. (1999). Early electric gun research. *IEEE Transactions on magnetics*, 35(1), 250-261. doi: https://doi.org/10.1109/20.738413

De Medeiros, L. H, Reyne, G. & Meunier, G. (1998). Comparison of global force calculations on permanent magnets. *IEEE Transactions on Magnetics,* 34(5), 3560-3563. doi: https://doi.org/10.1109/20.717840

Meeker, D. (2004). Finite element method magnetics: version 4.2 user's manual. Retrieved from http://www.femm.info/Archives/doc/manual.pdf.

Rashid, M. H. (2011). *Power electronics handbook: devices, circuits, and applications.* 3rd ed. USA: Elsevier.

Slade, W. G. (2005). A simple unified physical model for a reluctance accelerator. *IEEE Transactions on Magnetics,* 41(11), 4270-4276. doi: https://doi.org/10.1109/TMAG.2005.856320

Slade, W. G. (2006). Fast finite-element solver for a reluctance mass accelerator. *IEEE Transactions on Magnetics*, 42(9), 2184-2192. doi: https://doi.org/10.1109/TMAG.2006.880395